PHYSICAL REVIEW B **90**, 014419 (2014)

Different response of transport and magnetic properties of $BaIrO_3$ to chemical and physical pressure

M. A. Laguna-Marco,[1,2,*] G. Fabbris,[2,3] N. M. Souza-Neto,[2,4] S. Chikara,[2,5] J. S. Schilling,[3] G. Cao,[5] and D. Haskel[2,†]

[1]*Instituto de Ciencia de Materiales de Aragón and Departamento de Física de la Materia Condensada, CSIC-Universidad de Zaragoza, Zaragoza 50009, Spain*

[2]*Advanced Photon Source, Argonne National Laboratory, Argonne, Illinois 60439, USA*

[3]*Department of Physics, Washington University, St. Louis, Missouri 63130, USA*

[4]*Laboratorio Nacional de Luz Sincrotron (LNLS), Campinas, São Paulo 13083-970, Brazil*

[5]*Department of Physics and Astronomy, University of Kentucky, Lexington, Kentucky 40506, USA*

(Received 25 April 2014; revised manuscript received 21 June 2014; published 16 July 2014)

A combination of x-ray absorption, x-ray-diffraction, and transport measurements at high pressure is used to investigate the interplay between the electronic properties of Ir 5*d* states and lattice degrees of freedom in the weakly ferromagnetic insulator $BaIrO_3$. Although the Ir 5*d* *local* magnetic moment is highly stable against lattice compression, remaining nearly unperturbed to at least 30 GPa, the weak ferromagnetism (net ordered moment) is quickly quenched by 4.5 GPa (3% volume reduction). Under chemical pressure, where Sr is substituted for the larger Ba in $BaIrO_3$, the local magnetic moment on Ir remains stable, but the weak ferromagnetism is quenched after only 1.7% volume reduction. The magnetic ordering temperature T_m is also more strongly suppressed by chemical pressure compared to physical pressure. In addition, under ∼23-at. % Sr doping, $BaIrO_3$ undergoes a transition to a paramagnetic metallic state. Resistivity measurements indicate that $BaIrO_3$ remains an electrical insulator to at least 9 GPa, a much higher pressure than required to quench the weak ferromagnetism (∼4.5 GPa). Such a disparate response of transport and magnetic properties to chemical and physical pressure is likely rooted in the different compression rates of the (a,c) lattice parameters with Sr doping and applied pressure and the effect of related lattice distortions on electronic bandwidth and exchange interactions in this strongly spin-orbit-coupled system.

DOI: 10.1103/PhysRevB.90.014419 PACS number(s): 78.70.Dm, 75.47.Lx, 71.70.−d, 71.30.+h

I. INTRODUCTION

Traditionally, transition-metal oxides (TMOs) have attracted vast attention due to the rich variety of observed physical behaviors including high-T_C superconductivity [1], colossal magnetoresistance [2], and multiferroicity [3]. The plethora of ground states displayed by TMOs is rooted in the presence of competing interactions involving spin, charge, and orbital and lattice degrees of freedom. A consequence of such delicate balance is the ability to tune transport and magnetic properties of TMOs via external stimuli (temperature, pressure, electric and magnetic fields, uniaxial strain, optical excitation, etc). The large sensitivity of electron-electron interactions in these *d*-electron systems to changes in local chemical environment, symmetry, and dimensionality makes these compounds an attractive playground for the development of functional electronic and magnetic materials through manipulation on the nanoscale.

Lately, there has been a surge of interest in third-row (5*d*) TMOs due to the observation of localizedlike transport and magnetism in iridate compounds [4,5]. Since the spatial extent of the *d*-electronic wave function increases for $3d \rightarrow 5d$, the electronic and magnetic properties of 5*d* TM ions would be expected to display itinerantlike behavior due to the significant overlap of delocalized wave functions, rendering them weakly correlated wideband compounds. Experiments, however, show that strong spin-orbit (S-O) interactions in heavy 5*d* ions split the t_{2g} manifold created by the IrO_6 octahedral crystal electric field into $J_{\text{eff}} = \frac{1}{2}, \frac{3}{2}$ bands, the reduced bandwidth of the half-filled $J_{\text{eff}} = \frac{1}{2}$ band leading to a magnetically ordered insulating state via the relatively weak electron-electron interactions [4–6]. Spin-orbit interactions, then, drive 5*d* TMOs into a regime where crystal fields, electronic bandwidth, Coulomb, and exchange interactions have comparable energy scales, recovering the large sensitivity to external stimuli characteristic of the 3*d* counterparts. For example, $BaIrO_3$ is a magnetic insulator [7], whereas $SrIrO_3$ is a paramagnetic (PM) metal [8].

Within this context, further study of the layered iridate $BaIrO_3$ is especially interesting. The prominent role of S-O interactions in this material [9] and the strong coupling of magnetization to the lattice structure that follows present a unique opportunity for manipulating magnetism and transport via slight alterations in the crystal structure. $BaIrO_3$ is suggested to be a weak ferromagnet (FM) with a small net magnetic moment $\mu \approx 0.03\mu_B$/Ir [10], but a full description of the magnetic structure is still to be resolved. Its magnetic properties are found to be greatly sensitive to structural variations [7] with Sr doping drastically suppressing the magnetic ordering temperature T_m. Although the exact nature of its transport properties has been a matter of debate [11–14], it appears that $BaIrO_3$ is best characterized as an insulator on the verge of a metallic state [7,15]. Whereas short Ir-Ir distances across face-sharing octahedra allow direct Ir-Ir bonding and should favor broad 5*d* bands and itinerant behavior, rotations of corner-shared octahedra reduce bandwidth and stabilize an insulating state [7,15,16] (see Fig. 1). Doping Sr drives the system metallic, an indication that small distortions are sufficient to tune the electronic structure of $BaIrO_3$. An understanding of the structural changes introduced with Sr doping (chemical pressure introduced by replacing Ba^{2+} ions with smaller Sr^{2+}

*anlaguna@unizar.es
†haskel@aps.anl.gov

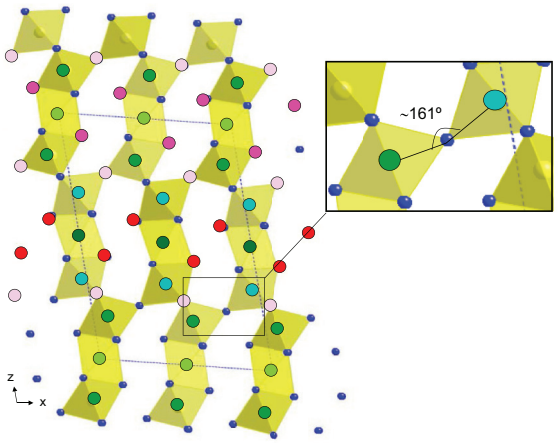

FIG. 1. (Color online) Schematic showing the nonequivalent Ir and Ba positions Ba1 (red), Ba2 (magenta), Ba3 (light pink), Ir1 (green), Ir2 (light green), Ir3 (cyan), and Ir4 (dark green). There are also six nonequivalent O positions, but they all have the same color for the sake of clarity. Note that several polytypes or polymorphs of $BaIrO_3$ may be formed, including multiphased samples containing a mixture of polytypes, depending on the synthesis conditions [17]. The crystal structure of our $BaIrO_3$ sample is similar to that of the nine-layered $BaRuO_3$, a 9R-layer polytype, but with a monoclinic distortion.

ions) and physical hydrostatic pressure and how these changes affect electronic structure and related magnetic and transport properties is highly desired. In addition to reducing lattice volume (isotropically or otherwise), pressure may induce distortions of IrO_6 octahedral units and/or their connectivity (i.e., changes in octahedral tilts affecting Ir-O-Ir angles), all bound to affect electronic structure, electron-electron correlations, and macroscopic properties.

In this paper, we have used x-ray absorption near-edge structure (XANES), x-ray magnetic circular dichroism (XMCD), x-ray-diffraction (XRD), and electrical resistivity measurements on $BaIrO_3$ at high physical pressure and extended x-ray absorption fine structure (EXAFS) on $Ba_{1-x}Sr_xIrO_3$ ($x = 0,0.06,0.12$) at ambient pressure, to gain a deeper insight into the delicate ground state of $BaIrO_3$ and the interplay between structural and electronic degrees of freedom. This study leverages previous results on the effect of Sr doping upon electronic structure and magnetism [9], which are referenced here for the purpose of comparing chemical and physical pressure. Whereas both internal and external pressure lead to the disappearance of weak ferromagnetism, the magnetic transition occurs at a larger unit-cell volume for chemical pressure indicating that it is not driven by a simple (isotropic) volume effect. Despite the loss of net magnetization, the Ir local magnetic moment, composed of a large orbital component [9], remains unchanged to at least 12-at. % Sr doping and 30 GPa, indicating that the disappearance of weak ferromagnetism is not due to a quenching of local magnetic moments, e.g., as a result of increasing crystal electric fields or band effects. Although chemical pressure yields a paramagnetic metal at ~23-at. % Sr doping, physical pressure stabilizes the insulating ground state. We argue that the different compression rates of (a,c) lattice parameters with chemical and physical pressure generate different lattice distortions driving the system more insulating under physical pressure and metallic under chemical pressure.

II. EXPERIMENT

Polycrystalline $BaIrO_3$ was synthesized using a solid-state reaction, whereas Sr-doped samples ($Ba_{1-x}Sr_xIrO_3$, $x = 0.06,0.12$) were grown as single crystals using the self-flux technique [7,13]. XRD measurements were carried out at the 16-BM-D beamline of the Advanced Photon Source (APS), Argonne National Laboratory (ANL). High-pressure XRD data were recorded at room temperature (RT) to 10 GPa. Fine powder (0.0008-in. mesh) was loaded into the sample chamber (210-μm hole in a stainless-steel gasket preindented to 60 μm) together with silicon oil as the quasihydrostatic pressure medium and silver powder as the *in situ* pressure calibrant. A copper-beryllium diamond-anvil cell (DAC) with 600-μm culet anvils was used for these measurements. Data were collected using x-ray radiation with $\lambda = 0.4245$ Å (29.21 keV) and a (3450 × 3450)-pixel Mar image plate. The two-dimensional diffractograms were integrated using the FIT2D program [18]. The diffraction patterns were Rietveld refined using the FULLPROF code [19].

The XANES/EXAFS/XMCD measurements were carried out at beamline 4-ID-D of the APS, ANL. EXAFS spectra were recorded at the Ir L_3 absorption edge on $Ba_{1-x}Sr_xIrO_3$ ($x = 0,0.06,0.12$) samples at ambient pressure as a function of temperature. XANES/XMCD spectra were recorded at the Ir $L_{2,3}$ absorption edges of $BaIrO_3$ as a function of temperature and pressure. Circularly polarized x rays were generated using phase-retarding optics [20,21]. XMCD was measured by switching x-ray helicity (12.7 Hz) and detecting the related modulation in the absorption coefficient with a lock-in amplifier [22]. The samples were field cooled in a 0.4-T field in order to align the weak ferromagnetic moment along the incident x-ray wave vector. Transmission geometry was used in all x-ray absorption measurements. Homogeneous layers of the sample were spread onto adhesive tapes for measurements at ambient pressure. High-pressure XMCD was performed using a copper-beryllium DAC fitted with 600-μm culet anvils and a nonmagnetic stainless-steel gasket. Powder was loaded into the sample chamber with silicon oil as the quasihydrostatic pressure transmitting medium and ruby powder for *in situ* pressure calibration. A low temperature was reached using a He-flow cryostat, and pressure was controlled remotely using a He-gas membrane. Further details on the implementation of the DAC environment in XMCD measurements can be found in Refs. [23,24].

Additional high-pressure room-temperature Ir $L_{2,3}$ XANES measurements were performed on $BaIrO_3$ at beamline 20-BM-B (Pacific Northwest Consortium/X-ray Science Division) of the APS, ANL. For this experiment, a symmetric cell ("Princeton University") was prepared with a partially perforated diamond anvil opposite a full diamond anvil both with 300-μm culet diameters bevelled to 180-μm culet diameters. A rhenium gasket was preindented to 30-μm, and a 80-μm-diameter hole was drilled in its center as a sample chamber. Neon gas was loaded as the pressure medium using the GSECARS/COMPRES system [25]. The powder

of $BaIrO_3$ was loaded together with a ruby ball, which was used as a pressure calibrant. XANES was measured in transmission mode, using (N_2/Ar)-filled ion chambers to detect incident/transmitted x-ray intensities.

The EXAFS spectra were analyzed according to standard procedures [26] using the HORAE-IFEFFIT (Athena, Artemis) program package [27,28]. For the analysis of the EXAFS spectra at the Ir L_3 edge, a cluster 7 Å in size was used in calculating theoretical standards. EXAFS data in the 3.00–14.00 $Å^{-1}$ k range (Hanning window, $dk = 0.2$ $Å^{-1}$) were Fourier transformed to real space. The half path lengths of the multiple-scattering (MS) paths involving the O and Ir atoms forming the intertrimer Ir-O-Ir angle (see Fig. 1) were parametrized in terms of the buckling angle and the single-scattering half path lengths in a similar manner to that described in Ref. [29]. In order to probe the effect of Sr doping on the Ir-O-Ir bonding angle, the high sensitivity of the scattering amplitude of nearly collinear Ir-O-Ir MS paths was exploited. This was performed by parametrization of the effective scattering amplitude $F_k(\theta)$ following the method proposed in Refs. [29,30]. Regarding the parameters for the sum-rule analysis of the x-ray absorption spectroscopy (XAS) and XMCD spectra, $n_h = 5$ has been used as the number of holes. A continuum edge step, modeled by an arctangent function centered at the absorption edge (taken as the inflection point on the rising edge) and defined to have unit height at the L_3 edge (0.5 at the L_2 edge), has been subtracted from the raw XAS data. The integrated intensity of the white line is then calculated over the range of energies where it is positive valued [i.e., from below the edge to the point where $\mu(E)$ first intersects the arctangent function]. For the magnetic dipole moment, $14\langle T_z\rangle/\langle 4S_z\rangle = 0.64$, obtained from the configuration-interaction calculations [9], has been used.

High-pressure four-point dc resistivity measurements were performed in a DAC prepared with diamonds with 500-μm culet diameters. A rhenium gasket was preindented to 100 μm, and a 250-μm-diameter hole was electrically drilled. The gasket was then insulated using a c-BN/Epoxy mixture, which also served as a nonhydrostatic pressure medium, and an ~150-μm sample chamber was dug using a needle. Leads cut from a thin Pt foil were used as electrical contacts. Additional details on the resistivity technique are given elsewhere [31]. Ruby fluorescence was used to calibrate pressure. The cell was loaded with a small $BaIrO_3$ single crystal, but, due to nonhydrostaticity and sample brittleness, the crystal was crushed as the cell was assembled, thus the presented data were powder averaged.

III. RESULTS

A. Electronic and magnetic characterizations

The branching ratio (BR) is defined as the ratio of the $L_{2,3}$ XANES white-line intensities, and it is proportional to the expectation value of the angular part of the spin-orbit interaction $\langle \mathbf{L}\cdot\mathbf{S}\rangle$ [32]. In the absence of core-valence Coulomb interactions, a statistical BR = 2 is obtained for a d band with a quenched orbital moment, and BR > 2 if $\langle \mathbf{L}\cdot\mathbf{S}\rangle \neq 0$ [9,32–34]. It has already been shown that BR ≈ 4.1 for $BaIrO_3$ at ambient pressure, and it remains

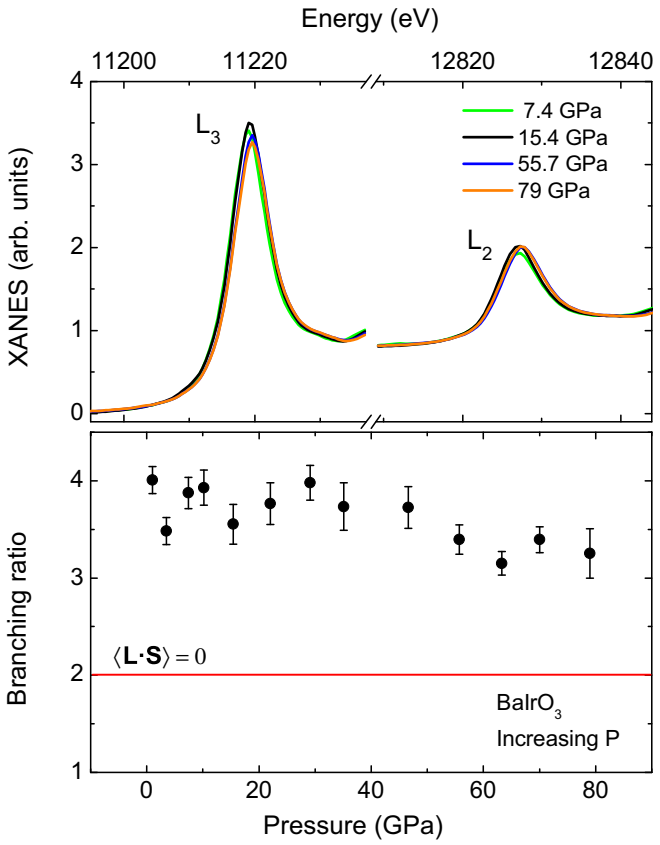

FIG. 2. (Color online) Ir $L_{2,3}$-edge XANES spectrum of $BaIrO_3$ recorded at room temperature and several external pressures up to ~79 GPa. Bottom: corresponding branching ratio.

unchanged with Sr doping up to at least 12 at. % [9]. The BR is also remarkably insensitive to pressure (see Fig. 2), remaining roughly constant up to 30 GPa and decreasing by less than 20% to 70 GPa. The BR indicates a remarkably stable $\langle \mathbf{L}\cdot\mathbf{S}\rangle$ (~2.1–1.9 in units of $\hbar^2$), whose strong effects are not eliminated by band effects even at 79 GPa.

In contrast to the BR stability, the XMCD signal is suppressed by both physical pressure (Fig. 3) and chemical pressure (Ref. [9]). In Fig. 3 a strong reduction in the XMCD intensity at 15 K at the Ir L_3 edge is clearly observed with increasing pressure. The XMCD intensity decreases by ~70% at 3.0 GPa, and no signal is observed above 4.5(5) GPa. The XMCD signal is proportional to the net magnetization, thus the mere absence of a signal at high pressure may be consistent with either a paramagnetic or a collinear antiferromagnetic (AFM) state. In principle, the disappearance of XMCD could also indicate a major change in the electronic structure of the 5d band, resulting in the disappearance of the local magnetic moment. However, we do not observe any significant change in L_3 or L_2 white-line intensities at low temperatures to 7 GPa, indicative of a stable branching ratio, in agreement with the observation at RT (Fig. 2). An unchanged BR value as high as 4.1 implies that $\langle \mathbf{L}\cdot\mathbf{S}\rangle$ remains unchanged at ~2.1–1.9, which is not compatible with a loss of local moment. The disappearance of weak ferromagnetism, then, is not the result of a loss of local magnetic moment as this would have yielded a significant change

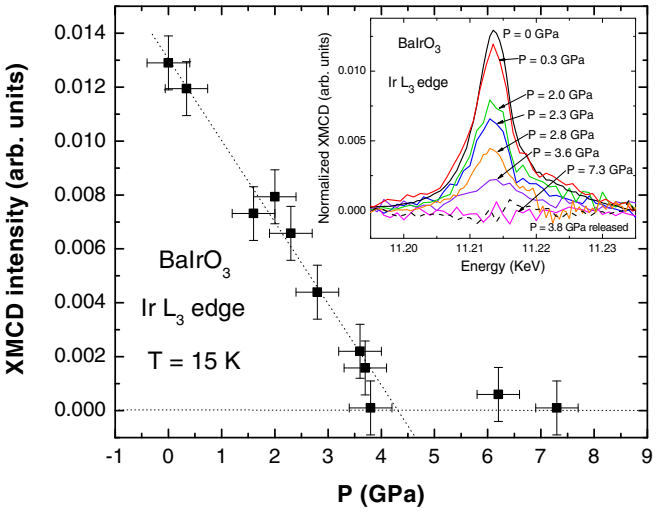

FIG. 3. (Color online) Intensity of the Ir L_3-edge XMCD spectrum of $BaIrO_3$ at $T = 15$ K, $H = 0.4$ T (after field cooling) as a function of the applied pressure. Inset: Ir L_3-edge XMCD spectrum of $BaIrO_3$ at $T = 15$ K, $H = 0.4$ T (after field cooling) as a function of the applied pressure. Only some of the spectra have been plotted for the sake of clarity. The XMCD signal recorded after releasing the gas out of the DAC membrane (3.8-GPa remanent pressure, shown in the inset as a dashed line) does not recover its initial intensity but stays at zero. This suggests that the effect of the applied pressure on the magnetic behavior is not completely reversible.

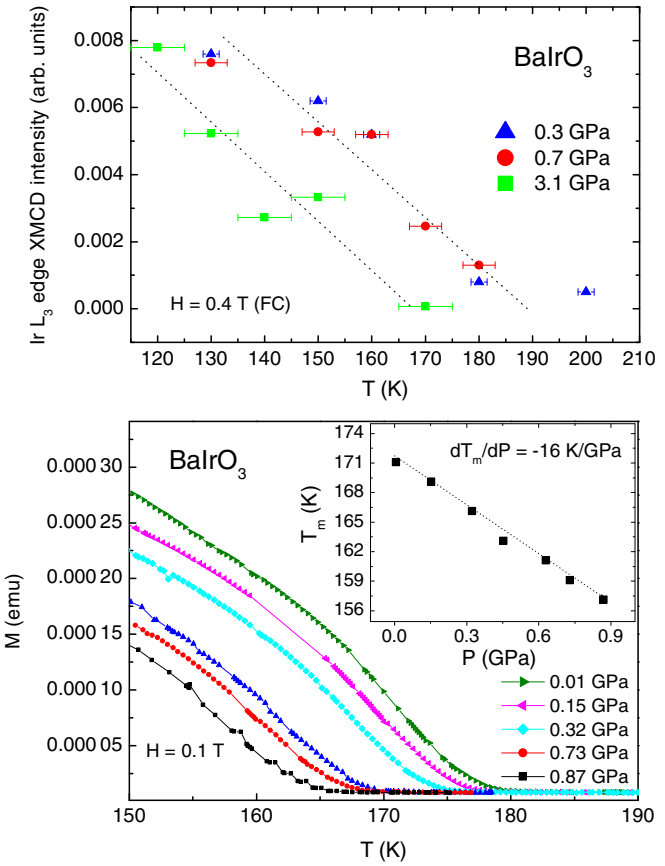

FIG. 4. (Color online) (Top) Intensity of the Ir L_3-edge XMCD spectrum of $BaIrO_3$ at $H = 0.4$ T (after field cooling) as a function of temperature for a few applied pressures. (Bottom) Magnetometry data at various pressures below 1 GPa with the inset showing the rate of T_m suppression with pressure.

in branching ratio, which is not observed. Moreover, the fact that the system remains an insulator under physical pressure with a relatively large ordering temperature (as shown below) is also indicative of the presence of robust local moments.

We note that under pressure T_m decreases at a much smaller rate than the saturation magnetization. For example, considering the XMCD data in the top panel of Fig. 4 and taking T_m for a given pressure as the midpoint value of XMCD(T) in the 130–190-K range, T_m remains nearly unchanged to 0.7 GPa, and a modest decrease is observed at 3.1 GPa, giving an estimated suppression rate of $-8(3)$ K/GPa (an $\sim$13% reduction at $\sim$3 GPa). For comparison, the related compound $SrRuO_3$ shows a $dT_m/dP \sim -5.7$ K/GPa [35]. The saturation magnetization, on the other hand, as measured by XMCD at $T = 15$ K, is reduced by 70% to 3 GPa (Fig. 3), a factor of 5.4 faster. A similar conclusion is obtained from the macroscopic magnetization data (lower panel of Fig. 4) where a $dT_m/dP \sim -16$-K/GPa suppression rate is found at 1 GPa, in reasonable agreement with the results of Kida *et al.* [36]. The reduction in T_m to 1 GPa is $\sim$8%, whereas the reduction in saturation magnetization is $\sim$48%, a factor of 6 faster.

As per the effect of chemical pressure, Refs. [7,9] show that the L_3 XMCD signal at $T = 5$ K decreases by $\sim$70% for 12% Sr doping (saturation magnetization decreasing from $\sim 0.027\mu_B$/Ir to $\sim 0.009\mu_B$/Ir), whereas T_m changes from $\sim$175 to $\sim$130 K, an $\sim$25% reduction (2.8 times slower than the saturation magnetization). Most importantly, the system becomes a paramagnetic metal at 23% Sr doping. In addition, sum rules [37,38] indicate that both L_z and S_z decrease at a similar rate, resulting in a nearly constant $L_z/S_z \sim 3$ ratio.

The pressure dependence of the electrical transport of $BaIrO_3$ is displayed in Fig. 5. At room temperature, a relatively small reduction in the resistance is observed at 8.8 GPa [39]. At low temperatures, on the other hand, R increases almost two orders of magnitude from 2.3 to 7.9 GPa (inset, Fig. 5). As for the temperature dependence of the resistance under applied pressure, it shows a negative slope throughout the whole temperature range (inset, Fig. 5). This result, together with the lack of a strong reduction in resistance with pressure, demonstrates that $BaIrO_3$ remains an insulator up to at least 8.8 GPa. Furthermore, the larger absolute slope observed at higher pressure suggests that the insulating gap is actually increasing within this pressure range. Overall the response of the electrical resistance to pressure is different from that found for Sr doping. Although chemical pressure continuously drives $BaIrO_3$ into a paramagnetic metallic state, which is reached at $\sim$23-at. % Sr doping [7], physical pressure drives it into a more insulating state. $BaIrO_3$ is an insulator below and above the magnetic transition observed at $\sim$4.5 GPa.

B. Structural characterization

Room-temperature high-pressure (up to 10 GPa) x-ray-powder-diffraction data were successfully indexed within the $C2/m$ space group with atomic positions as those proposed

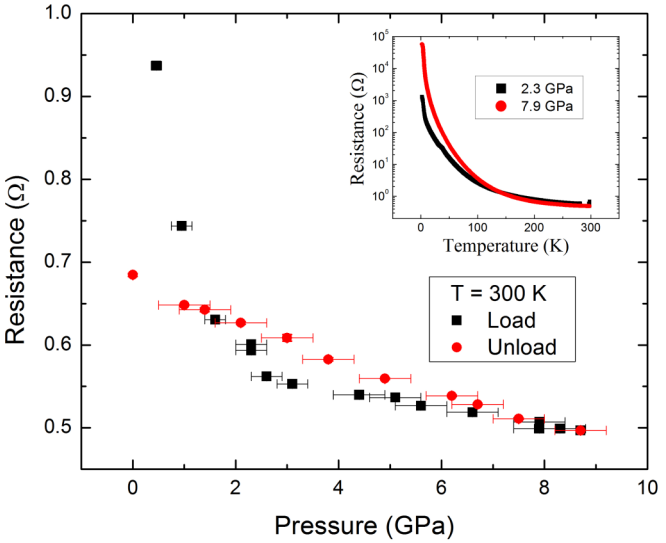

FIG. 5. (Color online) Pressure dependence of resistance in $BaIrO_3$. Only a small decrease in resistance is observed up to 8.8 GPa, indicating the persistence of the insulating state across the suppression of the XMCD signal (∼4.5 GPa). Such an insulating state is further demonstrated by the negative slope of the temperature-dependent resistance observed at 2.3 and 7.9 GPa (inset).

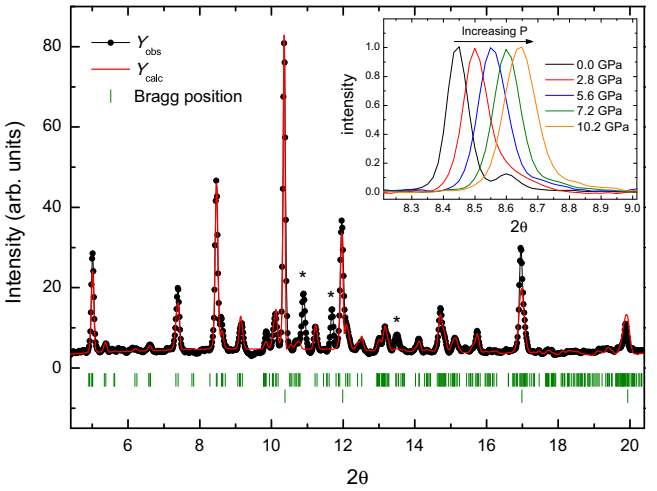

FIG. 6. (Color online) Observed (dots, black) and calculated (red solid line) XRD Rietveld profiles for $BaIrO_3$ at RT and 1.5 GPa. The first series of Bragg reflections correspond to the $BaIrO_3$ phase, and the second series correspond to the Ag powder used for calibration. Peaks marked with asterisks correspond to the DAC and do not change with pressure. The intensities of some of the peaks are not perfectly matched in the fit, likely due to a limited number of powder grains in the focused x-ray beam resulting in less than ideal powder averaging. The inset shows the shift of one of the reflections with increasing pressure.

by Siegrist and Chamberland [40]. A schematic of the crystal structure of ∼4.5 GPa can be seen in Fig. 1. It features three face-sharing IrO_6 octahedra forming Ir_3O_{12} clusters (trimer) that are vertex linked and tilted by 12° from one another to construct one-dimensional zigzag chains along the c axis. As a result, the Ir-O-Ir bonding angle is not 180° but is reduced to ∼161° as shown in the inset of Fig. 1 [41]. The Ba/Sr atoms are located in the channels outside the trimers. The local crystal structure around Ir is quite complex not only because there are four inequivalent Ir sites, but also because the octahedral environment around Ir atoms is quite distorted with either four or two distinct Ir-O distances.

As shown in Fig. 6, Rietveld refinement of the x-ray-diffraction patterns confirms the single-phase nature of the samples. In addition, no pressure-induced structural phase transitions were observed to 10 GPa. However, small distortions of oxygen atoms may go un-noticed in this powder-diffraction experiment due to the low scattering power of low-Z oxygen atoms. As seen in Fig. 7, room-temperature data show a linear dependence of the lattice parameters (a, b, c, and the volume of the unit cell) on applied pressure, which is reversible on pressure release. Previous room-temperature XRD studies on $(Ba,Sr)IrO_3$ compounds also showed a linear dependence of the lattice parameters on Sr doping [7]. A comparison of lattice volume contraction with physical and chemical pressure indicates that 12% Sr doping leads to the same volume contraction as ∼2-GPa applied pressure. However, the way the lattice contracts is different in both cases. Namely, for chemical pressure the a axis contracts at a faster rate than the c axis (for 12-at. % Sr doping $\Delta a/a_0 = -0.60\%$; $\Delta b/b_0 = -0.35\%$; $\Delta c/c_0 = -0.44\%$), whereas the opposite is the case with applied pressure [$(\Delta a/a_0)/\Delta P = -0.22(2)\%$/GPa; $(\Delta b/b_0)/\Delta P = -0.18(2)\%$/GPa; $(\Delta c/c_0)/\Delta P = -0.29(2)\%$/GPa].

To gain a deeper insight into the structural distortions induced by Sr doping, EXAFS spectra collected at ambient pressure have been analyzed. The Fourier transform of the EXAFS signal as a function of doping is displayed in the top panel of Fig. 8. The differences observed between the spectra are subtle. The EXAFS is particularly sensitive to distortions of three-body collinear arrangements from a 180° bond angle [30]. As seen in Fig. 8, simulations of EXAFS using

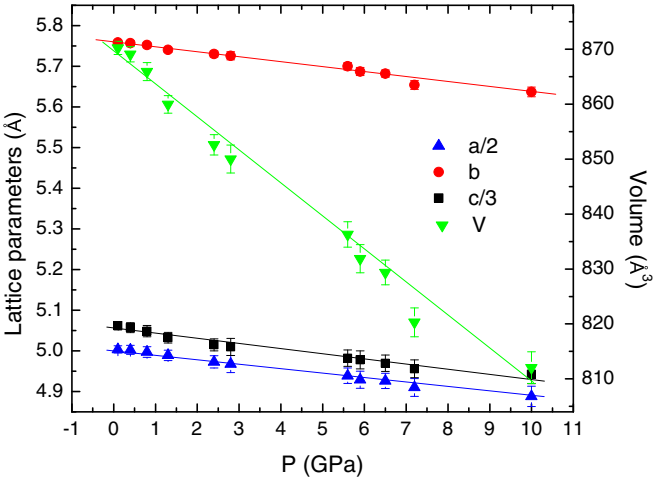

FIG. 7. (Color online) The lattice parameters a and b and the c axis (left axis) and volume (right axis) of the unit cell as a function of the applied pressure for $BaIrO_3$ at room temperature. The lattice parameters after releasing the pressure (data at 6.5 GPa) are also included. The values of a, b, and c after releasing the gas in the cell indicate that there is no irreversible (plastic) structural change.

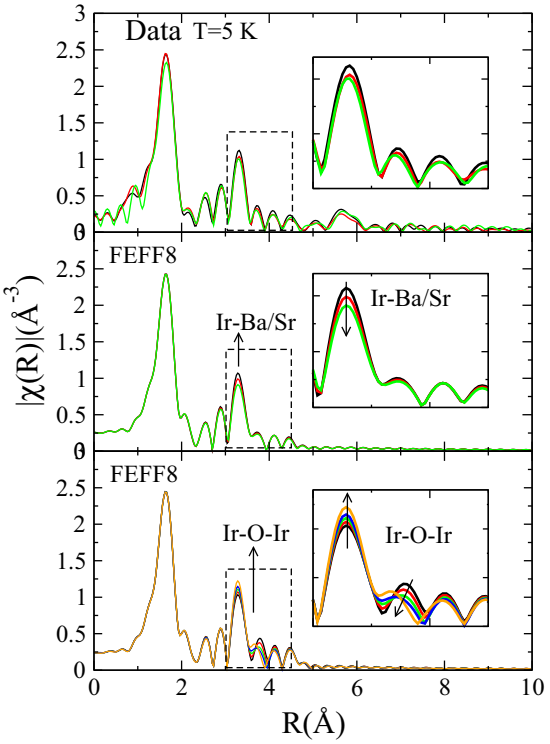

FIG. 8. (Color online) (Top) Doping (Sr) dependence of the Fourier-transformed EXAFS data. (Middle) FEFF8 simulations of the effect of doping Sr at Ba sites on the EXAFS signal arising from Ir-Ba/Sr scattering. $x = 0$ (black lines), $x = 0.06$ (red lines), and $x = 0.12$ (green lines). (Bottom) FEFF8 simulations of the effect of the changes in the Ir-O-Ir buckling angle on the Fourier transform for $\theta = 0^\circ$ (black lines), 10° (red lines), 15° (green lines), 19° (blue lines), and 25° (orange lines).

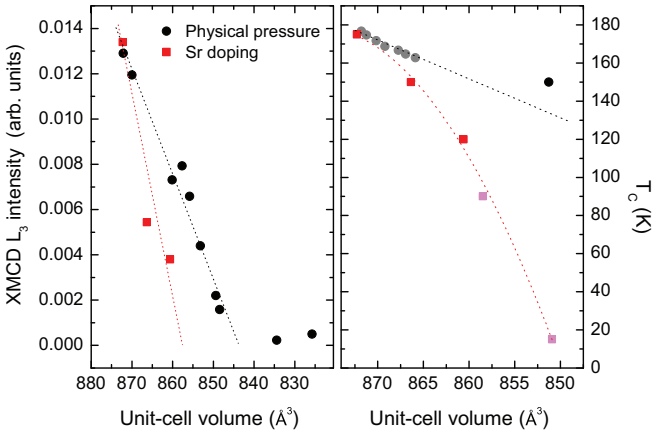

FIG. 9. (Color online) (Left panel) Intensity of the Ir L_3-edge XMCD spectrum of $BaIrO_3$ as a function of the applied pressure ($T = 15$ K and $H = 0.4$ T after field cooling) and (Ba,Sr)IrO_3 as a function of the Sr doping ($T = 5$ K and $H = 0.4$ T after field cooling). (Right panel) Modification of the T_m with applied pressure (circles) and Sr doping (squares). Red and black data were obtained from XMCD measurements, gray data and magenta data correspond to superconducting quantum interference device measurements (this paper and Ref. [7], respectively). Dotted lines are guides for the eye.

theoretical standards [42] show that the observed changes are mostly related to the replacement of Ba for Sr. In fact, a reduction in the Ir-O-Ir angle towards 180° would lead to data changes opposite to what is observed. Therefore, the modification of the EXAFS data with doping seems to be better explained in terms of the combined effect of Sr substitution plus a slight increase in the buckling angle ($< 5^\circ$; i.e., away from collinearity). The EXAFS data, hence, do not appear to support a picture in which the induced metallic state with doping is a result of a reduction in the Ir-O-Ir bond angle with doping.

IV. DISCUSSION

The Ir $L_{2,3}$ BR in $BaIrO_3$ and consequently the expectation value of the angular part of the spin-orbit interaction $\langle \mathbf{L} \cdot \mathbf{S} \rangle$ are remarkably stable for both physical and chemical pressure with ~30 GPa or 12-at. % Sr doping being insufficient to mix the S-O split $5d$ band and to alter the ($J_{\text{eff}} = 1/2$)-like state. The nearly pressure-independent branching ratio in $BaIrO_3$ suggests that little change to the $5d$ gap should occur. This is in agreement with our resistivity data to 8.8 GPa, which in fact, point to a small *increase* in the insulating gap. Similarly, the combined analysis of XANES and XMCD spectra indicates that the local (atomic) magnetic moment of $BaIrO_3$ is highly stable. Applying pressure, either chemical or physical, does not affect significatively the local moment, which keeps a sizable Ir $5d$ orbital moment as seen from the L_z/S_z ratio and the $\langle \mathbf{L} \cdot \mathbf{S} \rangle$.

On the other hand, the magnetic structure is more susceptible to either type of pressure, which drastically suppresses the amplitude of the XMCD signal. A comparison of the effect of physical and chemical pressure on the XMCD signal is shown in Fig. 9. Despite the XMCD signal being suppressed in both cases, chemical pressure does so more rapidly (see Fig. 9). Although a 70% reduction in XMCD intensity is observed at 12% Sr doping, the same volume contraction with pressure (at 2 GPa) results in a reduction of only ~45% (about 3 GPa of pressure are needed to obtain a 70% reduction). In terms of volume, the suppression of the magnetic ordering occurs at volume reduction values of 1.7% and 3.1% for chemical and physical pressure, respectively. In addition, the reduction in the ordering temperature is faster with chemical pressure: For instance, 6% Sr doping and 0.8 GPa pressure, both causing a 0.6% volume contraction, yield a 15% and 8% reduction in T_m, respectively. At ~851 Å^3 physical pressure reduces T_m by ~13% (27% if we consider the extrapolation from magnetization data), whereas chemical pressure reduces it by ~97%. Therefore, although the mere (isotropic) volume contraction appears to strongly contribute to the suppression of weak ferromagnetism, the disparate responses in transport and magnetism to either type of pressure (chemical and physical) indicate that the exact nature of the structural distortions in each case appears to play a key role.

Our electrical resistivity data indicate that the system becomes more insulating under pressure. By contrast, Sr doping leads towards a more metallic state with 23-at. % Sr doping resulting in a metal. It has been suggested that an increase in Ir-O-Ir collinearity with chemical pressure leads

to increased bandwidth, enhanced electron delocalization, and reduced magnetic interactions [7]. However, our EXAFS results appear to indicate that such an increase in collinearity does not take place. Furthermore, an (isotropic) volume effect is insufficient to explain the metallic state since $BaIrO_3$ remains an insulator to at least 8.8 GPa, which is equivalent to ~55-at. % Sr doping if unit-cell volumes are compared.

A key observation is the different ways in which the lattice parameters contract with chemical and physical pressure: a contracts faster than c for the former, whereas c contracts faster than a for the latter. The difference in the evolution of electronic properties with physical and chemical pressure must lie in the details of the Ir-O-Ir distortions. The delicate interplay between structural and electronic degrees of freedom has been recently reported on other related compounds. It has been shown that rare-earth (RE) doping also drives $BaIrO_3$ metallic through charge doping (REs are 3+), but around 1 GPa is sufficient to recover the insulating state in the doped samples [43]. The recovered insulating state was inferred to be related to a decrease in Ir-O-Ir angle. A similar increase in the insulating gap with pressure has been recently suggested to take place in Sr_2IrO_4 below ~10 GPa [44]. Although we are unable to provide detailed information on the nature of the Ir-O-Ir distortions, these should be measurable with either neutron powder diffraction and/or single-crystal x-ray diffraction, both as a function of Sr doping at ambient pressure, and to ~10 GPa for the parent compound.

The nature of the magnetic interactions in $(Ba,Sr)IrO_3$ is also a puzzling question. Unlike Sr_2IrO_4, the weak ferromagnetism of $BaIrO_3$ has been reported to be "intrinsic," i.e., due to a small local magnetic moment rather than to a canted antiferromagnetic coupling [10]. Whether this is the case or not remains to be determined, ideally by neutron-diffraction or x-ray resonant magnetic scattering measurements. A parallel alignment of the magnetic moments of the Ir atoms can be easily envisaged for those atoms within the same trimer (direct Ir-Ir exchange due to the short Ir-Ir bond length). However, for the Ir-O-Ir linkages of corner-sharing octahedra the superexchange interactions are expected to give rise to canted AFM coupling (canting being a result of antisymmetric superexchange associated with the deviation of Ir-O-Ir bonding from collinearity and the presence of a sizable spin-orbit interaction in $5d$ states). We have recently carried out an x-ray resonant magnetic scattering experiment on a single crystal of $BaIrO_3$ but, unfortunately, the results were inconclusive. No superstructure magnetic peaks could be observed. However, the absence of superstructure peaks does not disprove nor confirm the presence of antiparallel alignment of magnetic moments as the magnetic periodicity could coincide with the periodicity of the lattice. Although chemical pressure leads to a paramagnetic state, as clearly established in magnetometry measurements, the magnetic ground state of $BaIrO_3$ at high pressure remains elusive. The small reduction in T_m with physical pressure, despite a strong suppression of the net ordered moment, contrasts with the response of chemical pressure, which is characterized by a strong reduction in both the ordered moment and the T_m. This may indicate that the strength of magnetic interactions is not significantly reduced with pressure so the vanishing of the XMCD signal under pressure may well be related to a weak FM to collinear AFM transition if the faster c-lattice than a-lattice parameter contraction results in a reduction in Ir-O-Ir buckling with pressure. The effective moment measured in the paramagnetic state of $BaIrO_3$, $\mu_{\text{eff}} = 0.13\mu_B$, is much larger than the saturation magnetization in the ordered state $\mu_S = 0.027\mu_B$, providing further evidence that the weak ferromagnetism at ambient pressure is likely to originate in canting of an otherwise collinear AFM structure, a canting that is suppressed by 4.5 GPa. On the other hand, a reduction in Ir-O-Ir buckling with pressure is not easily reconciled with a concomitant increase in insulating character. Neutron-diffraction measurements may help to get more precise information about octahedral distortions and their relation to the magnetic structure.

Elucidating the nature of the magnetic interactions in $(Ba,Sr)IrO_3$ would also help clarify the relative importance of Coulomb and exchange interactions in driving gap formation in the ($J_{\text{eff}} = 1/2$)-like band. If the collapse of weak FM at ~4.5 GPa yields a PM state, the insulating character of $BaIrO_3$ at this pressure would imply that the electronic gap is not driven by magnetic exchange interactions but rather by on-site Coulomb interactions.

V. SUMMARY AND CONCLUSIONS

To summarize, the weakly ferromagnetic-insulating ground state of $BaIrO_3$ and its stability against physical compression were studied with element-specific and orbital-specific x-ray absorption spectroscopy, x-ray-diffraction, and transport measurements. The response of the electronic and magnetic degrees of freedom to pressure are compared to that obtained with chemical pressure (Sr doping at Ba sites) reported in previous papers [7,9]. Further insight on the effect of chemical pressure on the electronic properties of this compound is obtained here through Ir L_3 EXAFS measurements.

Pressure (both chemical and physical) barely affects the Ir $L_{2,3}$ BR, highlighting the robustness of the S-O split, the ($J_{\text{eff}} = 1/2$)-like ground state against lattice compression. On the other hand, both chemical and physical pressure strongly suppress the weak ferromagnetism in this compound. Chemical pressure does so more effectively for a given fractional volume change in the unit cell.

Furthermore, although chemical pressure quickly reduces the net ordered moment and ordering temperature for a given volume contraction, physical pressure reduces the ordered moment at a much faster rate than T_m, indicating that robust exchange interactions may remain present at high pressure. Whereas chemical pressure leads to a metallic state [7], physical pressure makes $BaIrO_3$ more insulating, at least up to 9 GPa. The different response of the electronic ground state to doping and physical pressure signals a strong interplay between structural and electronic degrees of freedom in $BaIrO_3$.

Our current results indicate that a uniform (isotropic) volume contraction alone cannot account for the disparate response in transport and magnetic properties of $BaIrO_3$ to chemical and physical pressure. Contrary to expectations, our EXAFS results do not support an increase in the Ir-O-Ir intertrimer angle towards 180° (more collinear) with Sr doping as the underlying mechanism for the Sr-driven insulator-metal transition. From our results it can be concluded that the

key for understanding the different effects of Sr doping and applied pressure on the magnetic and transport properties is the different way in which the lattice contracts with $|(\Delta a/a)/(\Delta c/c)| > 1$ (<1) for chemical (physical) pressure. Interestingly, we find that the reduction in XMCD intensity scales with the rate of contraction of the a-lattice parameter for both chemical and physical pressure.

ACKNOWLEDGMENTS

Work at Argonne is supported by the US Department of Energy, Office of Science, Office of Basic Energy Sciences, under Contract No. DE-AC-02-06CH11357. M. A. Laguna-Marco acknowledges Spanish MICINN for a postdoctoral grant and CSIC for a JAE-Doc contract. Research at Washington University was supported by the National Science Foundation (NSF) through Grant No. DMR-1104742 and by the Carnegie/DOE Alliance Center (CDAC) through NNSA/DOE Grant No. DE-FC52- 08NA28554. Work at the University of Kentucky was supported by the NSF through Grant No. DMR-1265162. The authors are grateful to H.-P. Liermann, Y.-C. Tseng, S. Heald, and M. Balasubramanian for support during HP-XRD, HP-XMCD, and HP-XANES measurements, respectively. We thank J. W. Kim for help with x-ray resonant magnetic scattering measurements. M. A. Laguna-Marco acknowledges M. C. Sánchez for her kind help with FULLPROF.

[1] J. G. Bednorz and K. A. Muller, Z. Phys. B **64**, 189 (1986).
[2] Y. Tokura and N. Nagaosa, Science **288**, 462 (2000).
[3] R. Ramesh and N. Spaldin, Nature Mater. **6**, 21 (2007).
[4] B. J. Kim, H. Jin, S. J. Moon, J.-Y. Kim, B.-G. Park, C. S. Leem, J. Yu, T. Noh, C. Kim, S.-J. Oh *et al.*, Phys. Rev. Lett. **101**, 076402 (2008).
[5] B. J. Kim, H. Ohsumi, T. Komesu, S. Sakai, T. Morita, H. Takagi, and T. Arima, Science **323**, 1329 (2009).
[6] G. Jackeli and G. Khaliullin, Phys. Rev. Lett. **102**, 017205 (2009).
[7] G. Cao, X. N. Lin, S. Chikara, V. Durairaj, and E. Elhami, Phys. Rev. B **69**, 174418 (2004).
[8] S. J. Moon, H. Jin, K. Kim, W. S. Choi, Y. S. Lee, J. Yu, G. Cao, A. Sumi, H. Funakubo, C. Bernhard *et al.*, Phys. Rev. Lett. **101**, 226402 (2008).
[9] M. A. Laguna-Marco, D. Haskel, N. Souza-Neto, J. C. Lang, V. V. Krishnamurthy, S. Chikara, G. Cao, and M. van Veenendaal, Phys. Rev. Lett. **105**, 216407 (2010).
[10] M. L. Brooks, S. J. Blundell, T. Lancaster, W. Hayes, F. L. Pratt, P. P. C. Frampton, and P. D. Battle, Phys. Rev. B **71**, 220411(R) (2005).
[11] R. Lindsay, W. Strange, B. L. Chamberland, and R. O. Moyer, Jr., Solid State Commun. **86**, 759 (1993).
[12] A. V. Powell and P. D. Battle, J. Alloys Compd. **191**, 313 (1993).
[13] G. Cao, J. E. Crow, R. P. Guertin, P. F. Henning, C. C. Homes, M. Strongin, D. N. Basov, and E. Lochner, Solid State Commun. **113**, 657 (2000).
[14] A. Ohnishi, M. Sasaki, Y. Kuroda, M. Sato, Y. Isobe, and G. Cao, Physica B **329–333**, 930 (2003).
[15] T. Nakano and I. Terasaki, Phys. Rev. B **73**, 195106 (2006).
[16] M. H. Whangbo and H. J. Koo, Solid State Commun. **118**, 491 (2001).
[17] B. Chamberland, J. Less-Common Met. **171**, 377 (1991).
[18] A. P. Hammersley, S. O. Svensson, M. Hanfland, A. N. Fitch, and D. Hausermann, High Pressure Res. **14**, 235 (1996).
[19] J. Rodriguez-Carvajal, Physica B **192**, 55 (1993).
[20] K. Hirano, K. Izumi, T. Ishikawa, S. Annaka, and S. Kikuta, Jpn. J. Appl. Phys., Part 2 **30**, L407 (1991).
[21] J. C. Lang and G. Srajer, Rev. Sci. Instrum. **66**, 1540 (1995).
[22] M. Suzuki, N. Kawamura, M. Mizumaki, A. Urta, H. Maruyama, S. Goto, and T. Ishikawa, Jpn. J. Appl. Phys., Part 2 **37**, L1488 (1998).
[23] D. Haskel, Y. C. Tseng, J. C. Lang, and S. Sinogeikin, Rev. Sci. Instrum. **78**, 083904 (2007).
[24] D. Haskel, Y. C. Tseng, N. M. Souza-Neto, J. C. Lang, S. Sinogeikin, Y. Mudryk, K. A. Gschneider, Jr., and V. K. Pecharsky, High Pressure Res. **28**, 185 (2008).
[25] M. Rivers, V. B. Prakapenka, A. Kubo, C. Pullins, C. M. Holl, and S. D. Jacobsen, High Pressure Res. **28**, 273 (2008).
[26] D. E. Sayers and B. Bunker, *X-Ray Absorption: Principles, Applications, Techniques of EXAFS, SEXAFS, and XANES* (Wiley, New York, 1988), Chap. 6.
[27] M. Newville, J. Synchrotron Radiat. **8**, 322 (2001).
[28] B. Ravel and M. Newville, J. Synchrotron Radiat. **12**, 537 (2005).
[29] D. Haskel, Ph.D. thesis, University of Washington, 1998.
[30] D. Haskel, E. A. Stern, F. Dogan, and A. R. Moodenbaugh, Phys. Rev. B **61**, 7055 (2000).
[31] K. Shimizu, K. Amaya, and N. Suzuki, J. Phys. Soc. Jpn. **74**, 1345 (2005).
[32] G. van der Laan and B. T. Thole, Phys. Rev. Lett. **60**, 1977 (1988).
[33] D. Haskel, G. Fabbris, M. Zhernenkov, P. P. Kong, C. Q. Jin, G. Cao, and M. van Veenendaal, Phys. Rev. Lett. **109**, 027204 (2012).
[34] J. P. Clancy, N. Chen, C. Y. Kim, W. F. Chen, K. W. Plumb, B. C. Jeon, T. W. Noh, and Y. J. Kim, Phys. Rev. B **86**, 195131 (2012).
[35] J. J. Neumeier, A. L. Cornelius, and J. S. Schilling, Physica B **198**, 324 (1994).
[36] T. Kida, A. Senda, S. Yoshii, M. Hagiwara, T. Nakano, and I. Terasaki, J. Phys.: Conf. Ser. **200**, 012084 (2010).
[37] B. T. Thole, P. Carra, F. Sette, and G. van der Laan, Phys. Rev. Lett. **68**, 1943 (1992).
[38] P. Carra, B. T. Thole, M. Altarelli, and X. Wang, Phys. Rev. Lett. **70**, 694 (1993).
[39] Note that the reduction in resistance by $\sim 1/2$ from ambient pressure to 2 GPa upon pressure loading is likely to be due to improved contact between the powder grains; this is further evidenced by the unrecovered resistance obtained upon pressure unloading.
[40] T. Siegrist and B. Chamberland, J. Less-Common Met. **170**, 93 (1991).

[41] According to the unit cell proposed by Siegrist and Chamberland, there are two different Ir-O-Ir angles: $180 - \theta \sim 180 - 19.1$ and $180 - \theta' \sim 180 - 16.4$. In the simulation the change in the angles has been linked: $\theta' = \theta \times 0.86$.

[42] A. L. Ankudinov, B. Ravel, J. J. Rehr, and S. D. Conradson, Phys. Rev. B **58**, 7565 (1998).

[43] O. B. Korneta, S. Chikara, S. Parkin, L. E. DeLong, P. Schlottmann, and G. Cao, Phys. Rev. B **81**, 045101 (2010).

[44] D. A. Zocco, J. J. Hamlin, B. D. White, B. J. Kim, J. R. Jeffries, S. T. Weir, Y. K. Vohra, J. W. Allen, and M. B. Maple, J. Phys.: Condens. Matter **26**, 255603 (2014).